Med Biol Eng Comput
DOI 10.1007/s11517-009-0466-8

ORIGINAL ARTICLE

3D-patient-specific geometry of the muscles involved in knee motion from selected MRI images

I. Südhoff · J. A. de Guise · A. Nordez · E. Jolivet · D. Bonneau · V. Khoury · W. Skalli

Received: 18 December 2007 / Accepted: 12 February 2009

Abstract Patient-specific muscle geometry is not only an interesting clinical tool to evaluate different pathologies and treatments, but also provides an essential input data to more realistic musculoskeletal models. The protocol set up in our study provided the 3D-patient-specific geometry of the 13 main muscles involved in the knee joint motion from a few selected magnetic resonance images (MRIs). The contours of the muscles were identified on five to seven MRI axial slices. A parametric-specific object was then constructed for each muscle and deformed to fit those contours. The 13 muscles were obtained within 1 h, with less than 5% volume error and 5 mm point-surface error (2RMS). From this geometry, muscle volumes and volumic fractions of asymptomatic and anterior cruciate ligament deficient subjects could easily be computed and compared to previous studies. This protocol provides an interesting precision/time trade-off to obtain patient-specific muscular geometry.

I. Südhoff (✉) · A. Nordez · E. Jolivet · D. Bonneau · W. Skalli (✉)
Laboratoire de biomécanique, Arts et Metiers Paristech, CNRS, 151 Boulevard de l'hopital, 75013 Paris, France
e-mail: isudhoff@yahoo.fr

W. Skalli
e-mail: wafa.skalli@paris.ensam.fr

I. Südhoff · J. A. de Guise
Laboratoire de recherche en imagerie et orthopédie, Centre de recherche du CHUM, École de technologie supérieure, Montreal, QC, Canada

J. A. de Guise · V. Khoury
Centre Hospitalier de l'Université de Montréal, Montreal, QC, Canada

Keywords Muscles · Patient specific · Geometry · Knee · MRI

1 Introduction

The need for estimating precisely the patient-specific muscle geometry is twofold. First, it represents an essential input data for musculoskeletal models, which are often based on scaled cadaveric measurements. The need to individualize the geometry of those models has been recently highlighted by several authors [3, 5, 27]. Secondly, the patient-specific geometry (and thereby also the volume, lever arm etc) provides an important clinical data to evaluate different pathologies and the outcomes of the treatments used. For example, the morphology of the gastrocnemius in hemiplegic cerebral palsy patients [18], the muscle–tendon geometry after rectus femoris tendon transfer [4], and the quadriceps femoris muscle morphology after anterior cruciate ligament (ACL) injury [26] have recently been investigated. The volume of the muscles, which can be derived from their geometry, is also clinically relevant to assess the atrophy or hypertrophy resulting from different pathologies, treatments, and strength training [1, 2, 15, 17, 25]. The ratio between the volume of the quadriceps and the hamstrings is also a useful tool to investigate the muscular function of ACL deficient subjects [26].

To obtain the individualized 3D geometry, cross-sectional area of the muscles can be identified on a set of continuous axial magnetic resonance images (MRI). Semi-automated or fully automated segmentation methods are inefficient because muscle distinction is often difficult or impossible to assess using currently used methods. Thus, manual muscle contour is the most used method to obtain muscle volume [4, 6, 10]. This method is time-consuming,

Published online: 10 March 2009

limiting thereby its clinical application. Other authors [7, 23] obtain the 3D-geometry by deforming a generic object. However, with a reduced number of muscle contours on MRI slices (i.e., in parallel planes), there is not enough information to describe efficiently a non-linear deformation in the 3D-space. This leads to inaccurate muscle models. To improve such methods, a large number of muscle contours has to be used to increase the geometrical information that determines the deformation.

Considering the lack of a clinically usable method to obtain patient-specific 3D geometry of the muscles at the hip, Jolivet and colleagues [12, 13] recently developed a method based on the deformation of a parametric specific object (DPSO) to assess muscle geometry with a reduced number of axial images. It consists of characterizing each muscle contour by a parametric ellipse and interpolating the parameters of the ellipses to build a regular surface mesh. This approximate object and the corresponding mesh are then deformed to fit the exact contours of the muscles yielding subject-specific geometry using a non-isotropic kriging algorithm [24]. This technique determines the volumes and the shapes of the gluteus maximus, gluteus medius, gluteus minimus, fascia lata tensor and sartorius muscles using five to six slices with a satisfactory accuracy (average absolute volume error of 2.4% comparing to the volume obtained with all available slices). Jolivet et al. [13] described this technique for the hip muscles and only considered two different subsets of images (three to four or five to six slices, depending on the muscles) to assess the precision of the method. Moreover, this method was four times faster than the method using all available slices to generate the volume of the muscle [13].

The objective of this work was to adapt the DPSO method and propose a protocol to get the 3D-patient-specific geometry of the 13 main muscles involved in the knee joint motion. The selection of the necessary slices to obtain a given accuracy and the reproducibility of the protocol are investigated. A preliminary clinical research application provides the volume of the muscles for ten asymptomatic subjects and five subjects waiting for an ACL reconstruction to investigate the difference in muscle volume distribution between these two groups.

2 Materials and methods

2.1 Subjects

Ten asymptomatic young men [29 (SD 4) years, height 177 (SD 6) cm, weight 75 (SD 8) kg and 5 young men waiting for an ACL reconstruction 29 (SD 2) years, height 176 (SD 7) cm, weight 78 (SD 11) kg, time since ligament rupture >11 months] consented to participate in the protocol previously approved by institutional ethic committees[1]. Asymptomatic subjects practiced recreational sports, but did not participate in any strength training at the time of the study.

2.2 Magnetic resonance imaging

A Siemens Avanto 1.5 T MRI scanner was used to obtain three series of axial images from the iliac spines to the calcaneus (slice thickness 4 mm, gap 0 mm, resolution 0.78 mm × 0.78 mm). The VIBE (Volume Interpolated GRE) sequence was chosen in order to obtain good quality images of the muscles of the lower limb in a reasonable time (6 min per series). An angiography radio-frequency coil was used so as to encompass the entire lower limb. Three hundred images were thereby acquired for each subject.

2.3 Identification of muscles

According to previous studies [16, 19] and functional considerations, the following 12 muscles involved in the knee joint motion were considered: semimembranosus (SM), semitendinosus (ST), biceps femoris long head (BFL), biceps femoris short head (BFS), sartorius (SAR), tensor fascia latae (TFL), gracilis (GRA), vastus lateralis and vastus intermedius (VIL), vastus medialis (VM), rectus femoris (RF), medial gastrocnemius (MG), and lateral gastrocnemius (LG). VIL was in fact a combination of vastus intermedius and vastus lateralis because they are very difficult to distinguish from each other and they have the same function. Using a specific software developed by the laboratory of biomechanics (AM ParisTech), each muscle contour was manually identified. Each muscle was outlined on the images by manually picking points on the outline of the muscle. A spline was computed using already picked points. The last picked point had to be close to the first picked point in order to get a closed contour. [13].

2.4 Reference models

To assess the error of our protocol, a reference model was defined using a complete set of N slices for two asymptomatic subjects, randomly selected. Each muscle contour was identified on all the 300 continuous images by one operator (12 h were required for each subject). These contours led, for each subject, to a 3D-model of each muscle, which was considered as the reference model (see

[1] Ecole de Technologie Supérieure de Montréal, Centre Hospitalier de l'Université de Montréal, Hôpital du Sacré Cœur de Montréal, Centre de Recherche interdisciplinaire en réadaptation du Montréal métropolitain, Hôpital Maisonneuve-Rosemont de Montréal.

Fig. 1). The error in volume was computed as the difference between the reference model and the muscle reconstruction with the DPSO method. The error in shape was assessed by computing the point-surface error calculated as the distance between each point of the muscle reconstruction with the DPSO method and its projection on the surface of the corresponding reference model. Ninety-five percent of these distances are below the computed root mean square (2RMS) point to surface distance error [20, 21].

To evaluate the inter-observer reproducibility of those reference models, one of the subjects was also reconstructed by a second operator. The volume error between the reconstructions of both operators remained under 17 cm^3 except for LG (the difference reached 41 cm^3, i.e., 24% of the muscle volume). This represented less than 6% of the muscle volume, except for the BFS, SAR, GRA (10%). The reproducibility of the muscle shape was acceptable (mean point-surface error <1 mm; 2RMS <3 mm).

2.5 Assessment of the optimal number of slices

A preliminary study was performed to assess the optimal number of slices to obtain accurate muscle geometry. A subset of 4–22 regularly spaced slices were used to reconstruct the muscles of the two subjects with the DPSO method. The precision of the reconstructions was assessed by comparing their shape (point-surface distance) and volume to the reference models.

The volume error with respect to the volume obtained using reference models should be decreased if the number of slices used for the reconstruction is increased. Therefore, the smallest number of slices providing a reconstruction with a given threshold of *n%* for the volume error was determined for subjects 1 (*n1*) and subject 2 (*n2*). The optimal number of slice $NS_{optn\%}$ was defined as $NS_{optn\%} = \max(n1, n2) + 1$. $NS_{optn\%}$ is used for all future reconstructions performed with the DPSO method.

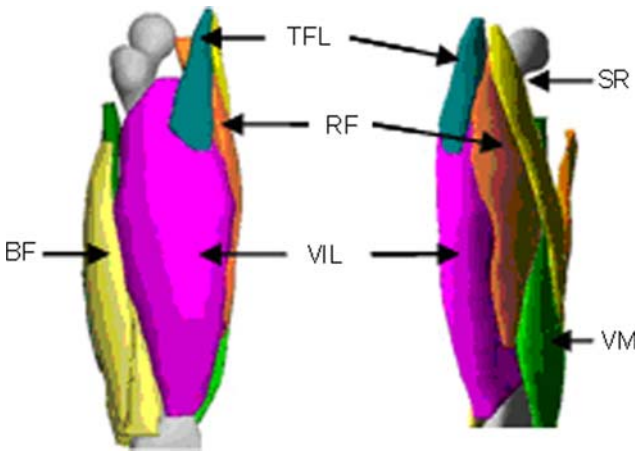

Fig. 1 Typical 3D-patient-specific geometry of the thigh muscles: *BF* biceps femoris, *SAR* sartorius, *TFL* tensor fascia latae, *VIL* vastus lateralis and intermedius, *VM* vastus medialis, *RF* rectus femoris

2.6 Reconstruction protocol

The protocol was defined as follows: the operator identifies the upper and the lower limits of each muscle. These limits correspond to the slices of the musculo-tendineous junction, i.e. where the contractile tissue (muscle) becomes fibreous (tendon). From $NS_{optn\%}$ and the upper and lower limits, a program computes the slice numbers on which each muscle has to be identified. For each muscle, the operator is given a list of $NS_{optn\%}$ slices to treat. Therefore, the 3D-geometry of each muscle is then obtained from the $NS_{opt5\%}$ slices using the previously described algorithm [12, 13]. Briefly, this algorithm could be decomposed in three steps. (1) The $NS_{opt5\%}$ muscle contours were modeled as equivalent ellipses. The coordinates of the centroid, local inertial coordinate systems, width, and length were calculated for the $NS_{opt5\%}$ available ellipses. (2) Changes in these parameters along the muscle's principal axis were modeled using a cubic spline interpolation to estimate missing ellipses. Using all available and estimated ellipses, the resulting 3D parametric object was reconstructed. (3) The subject-specific volumic muscle reconstruction was obtained by deforming the parametric object using a non-isotropic algorithm [24] and the $NS_{opt5\%}$ available muscle contours.

2.7 Reproducibility of muscle reconstruction with the DPSO method

The study presented in this paragraph aimed at assessing the inter-observer reproducibility of the muscle geometry obtained with the DPSO method using $NS_{optn\%}$ slices (determined for each muscle). Twelve muscles of 10 asymptomatic subjects were reconstructed by two operators. The difference in shape and volume between both reconstructions was assessed. The relative volume reproducibility was defined as the absolute difference in volume of the reconstructions, divided by the volume of the reconstructions of the first operator. The mean difference and the standard deviation (SD) of this relative volume error were computed for each muscle. The interclass correlation coefficient (ICC) was calculated [11]. The shape reproducibility was assessed by computing the point-surface error and 2RMS of this distance were calculated.

2.8 Preliminary clinical research application research

The 12 muscles of 5 anterior cruciate ligament deficient (ACLD) subjects were also reconstructed by using the

previously described protocol (with a volume threshold equal to 5%). The volume of the muscles and the volumic fraction (muscle volume divided by the volume of all the muscles, as described by [9, 13]) were calculated for both asymptomatic and ACLD subjects.

3 Results

3.1 Assessment of the optimal number of slices

The accuracy of the reconstructions (volume difference with respect to the volume obtained using reference models) for different subsets of images of one operator is shown in Fig. 2. The reconstruction errors of the muscles differed among muscles when less than seven slices were used. The optimal number of slices $NS_{opt5\%}$ to obtain an error inferior to 5%, varied from five to seven slices depending on the muscle. When using more than seven slices, the volume error with respect to the reference models still diminished to finally reach 2% with 22 slices.

With more than seven slices, the point-surface error (see Fig. 3) was less than 5 mm (2RMS). This error diminished when even more slices were used: with 13 slices, it reached 2 mm.

The maximal difference between *n1* and *n2* was one slice. The values of $NS_{opt5\%}$, and volume and point-surface errors obtained for the two subjects using $NS_{opt5\%}$ slices are provided in Table 1.

3.2 Reproducibility of muscle reconstruction using the DPSO method

Considering a threshold of 5%, the reconstruction of 12 muscles of a subject with a reduced set of slices took about 1 h (compared to more than 12 h when using all the slices). The difference between the volume and shape of the muscles reconstructed by the two operators is shown in Table 2. The mean muscle volume, the minimal and maximal values obtained among the ten reconstructed subjects for the point-surface (2RMS) error are also provided. The error in reproducibility was very variable depending on the reconstructed muscles. For example, for BFS muscle, the relative mean error reached 10.8% among subjects, corresponding to an absolute mean error of 11.9 cm^3. The biggest absolute (29.4 cm^3) and smallest relative error (1.9%) was observed for VIL. The point-surface errors remained in a confidence interval between ±2.7 and ±6.3 mm (2RMS) for all muscles. The biggest confidence intervals were found for the *gastrocnemii* (±6.3 mm for the MG and ±6.1 mm for the LG). For all muscles the ICC was >0.85.

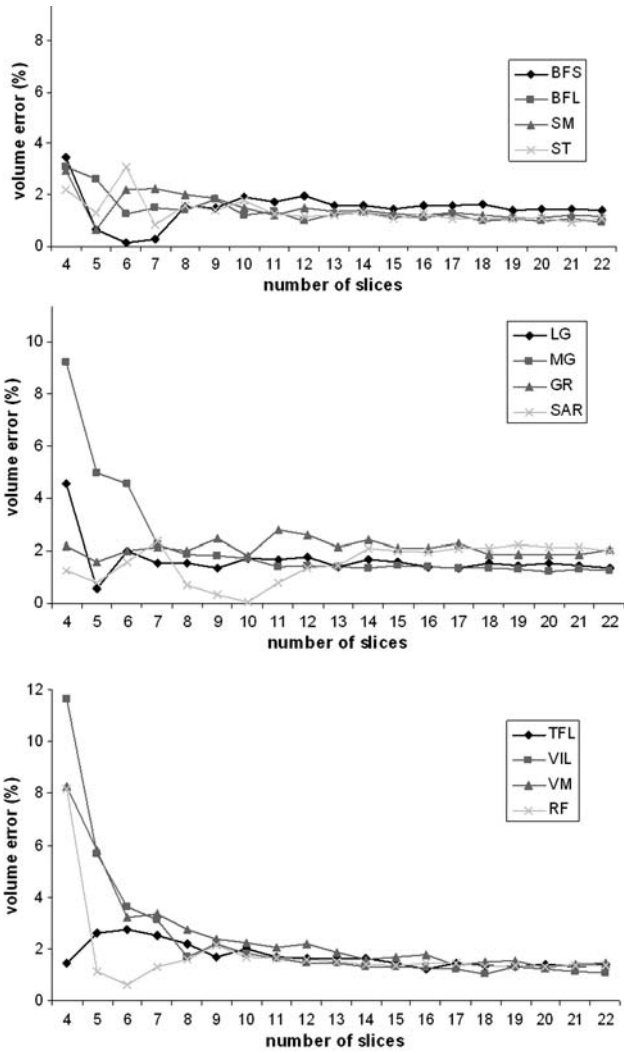

Fig. 2 Volume error (compared to the reference models) for the 12 reconstructed muscles in one subject (reconstructed by one operator)

3.3 Preliminary clinical research application

The boxplots of the volume and the volumic fraction of the 12 muscles of asymptomatic and ACL deficient subjects are shown Figs. 4 and 5. The VIL muscle was the largest muscle, with a mean volume of about 1,500 cm^3, ranging from 1,165 to 2,002 cm^3. This corresponded to 36% of the global muscular volume. The vastus medialis and rectus femoris volume reached about 550 and 340 cm^3, representing respectively about 13 and 8% of the global muscular volume. BFL, SAR, SM, and ST contributed 5–6% of the global volume. The gastrocnemius muscles (LG and MG) represented 10–12% of the muscular volume. The smallest muscles were BFS, GRA and TFL, with a volumic fraction of <3%.

The mean volume of the VM, BFS and BFL muscles were bigger for the ACL deficient subjects than for the asymptomatic subjects. The opposite was observed for the

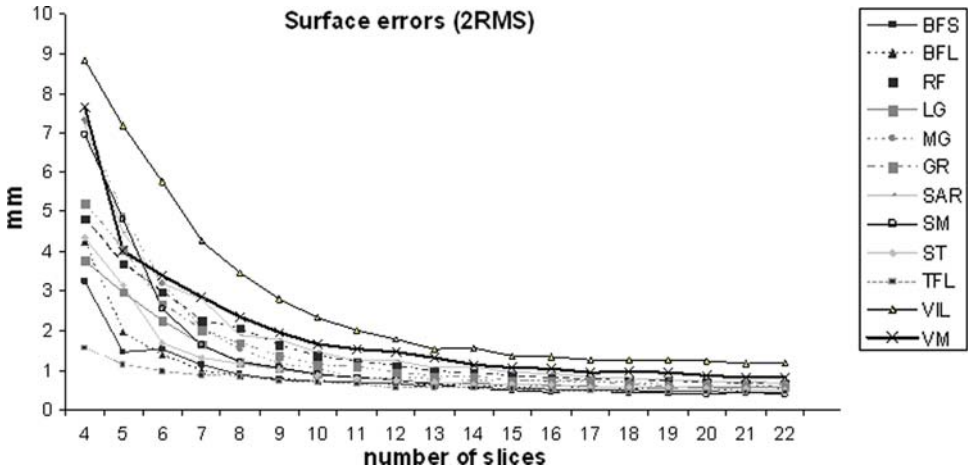

Fig. 3 Surface error (2RMS) for the 12 reconstructed muscles in one subject (reconstructed by one operator)

Table 1 Optimal number of slices ($NS_{opt5\%}$) used to obtain the 3D-geometry with a volume error <5% with respect to the volume obtained using reference models

Muscles	Optimal number of slices	Volume error (%)		Point-surface error (mm)	
		Subject 1	Subject 2	Subject 1	Subject 2
BFS	8	4.17	1.56	2.40	0.90
BFL	6	1.22	1.28	1.60	1.39
RF	6	0.3	0.60	3.60	2.98
LG	6	0.74	2.01	2.40	2.26
MG	8	3.28	1.86	3.31	1.53
GRA	7	3.27	2.13	2.51	2.02
SAR	7	2.87	2.37	3.49	2.80
SM	6	1.29	2.18	1.81	2.57
ST	6	3.55	3.06	3.06	1.68
TFL	6	2.02	2.73	1.29	0.96
VIL	7	2.42	3.12	4.89	4.28
VM	7	2.89	3.35	3.92	2.85
Total	80				

Volume and point-surface errors obtained using the optimal number of slices for the two subjects

SM semimembranosus, *ST* semitendinosus, *BFL* biceps femoris long head, *BFS* biceps femoris short head, *SAR* sartorius, *TFL* tensor fascia latae, *GRA* gracilis, *VIL* vasti lateralis and intermedius, *VM* vastus medialis, *RF* rectus femoris, *MG* medial gastrocnemius, and *LG* lateral gastrocnemius

ST and SAR muscles. The ACL deficient subjects had a bigger variability in muscle volume than asymptomatic subjects. The RF and VIL volumes were similar between populations.

4 Discussion

This study led to a clinically feasible method to reconstruct the patient-specific-3D geometry of the 12 main muscles involved in the knee joint motion from MRI in 1 h.

4.1 Identification of muscles

Some limitations had to be dealt with. First, differentiating some of the muscles was very difficult in some parts of the thigh or shank, as the epimysium was not always clear enough to identify on the images. For example, the *gastrocnemii* muscles were difficult to differentiate at the mid-thigh, and the vastus medialis was difficult to differentiate from the vastus intermedius at the proximal part of the thigh. Other authors have reported similar difficulties [1, 14]. Moreover, the upper and lower limits were difficult to define very accurately, as the transition from muscular to fibrous tissue is progressive. To quantify the influence of the subjective upper and lower limits definitions on the reconstructions of the muscles, we looked at the residual volume. This residual volume was comprised between the upper limits and lower limits of two operators. Between the two operators, these limits differed by zero to five slices, depending on the considered muscle (mean across subjects <2.9 slices; Table 3). This averaged residual volume ranged from 0.2% (ST) to 2.1% (BFS) (Table 3), and was small compared to the volume reproducibility between the reconstructions of two operators. Considering the reliability of the reference models (for most muscles the volume error between both operators reference muscle reconstructions represented <6% of the muscle volume), it seemed that the threshold of 5% for the volume error with respect to the volume obtained using reference models represented a good trade-off between the required precision to match the reported intra-observer variability and the analysis time required to outline the muscles on the images.

4.2 Reference models and reproducibility of the protocol

For the reproducibility of the reference models, we obtained 6% of volume error between both operators

Table 2 Difference in volume (in percent and cubic millimeter) and shape (point surface error in millimeter) between the muscles reconstructed by two operators

	BFS	BFL	RF	LG	MG	GRA	SAR	SM	ST	TFL	VIL	VM
Volume error												
Mean (%)	10.8	5.9	4.9	7.1	5.6	8.6	8.4	5.8	7.5	4.3	1.9	3.2
2SD (%)	10.6	5.6	4.3	13.9	8.9	5.2	10.9	5.4	6.5	6.0	2.7	3.4
Mean (mm^3)	11,908	14,786	17,183	13,988	18,049	11,090	19,049	14,692	18,345	3,197	29,359	17,988
2SD (mm^3)	11,803	17,151	17,361	32,238	37,253	7,230	25,045	12,112	15,331	4,372	52,159	22,997
ICC	0.96	0.99	0.98	0.86	0.96	0.99	0.93	0.99	0.96	0.98	0.99	0.99
Mean volume (mm^3)	115,126	233,962	344,366	197,148	307,404	130,589	220,440	261,791	245,928	77,853	1,477,661	542,664
Point-surface error												
Global 2RMS	2.7	3.3	3.4	6.1	6.3	3.1	3.6	2.8	2.7	3.1	5.6	3.7
Minimum (2RMS)	1.8	1.7	1.6	2.8	2.5	1.3	1.3	1.8	1.2	1.4	2.0	2.1
Maximum (2RMS)	3.8	5.8	7.1	10.8	14.3	6.9	7.6	4.3	3.5	5.6	8.4	4.8

Mean and standard deviation (SD) are computed among ten subjects, with the relative errors in volume between two reconstructions. Point-surface errors are presented with the 2RMS of the distance for all subjects (with minimum and maximum values for the 2RMS of the distance)

SM semimembranosus, *ST* semitendinosus, *BFL* biceps femoris long head, *BFS* biceps femoris short head, *SAR* sartorius, *TFL* tensor fascia latae, *GRA* gracilis, *VIL* vasti lateralis and intermedius, *VM* vastus medialis, *RF* rectus femoris, *MG* medial gastrocnemius, and *LG* lateral gastrocnemius

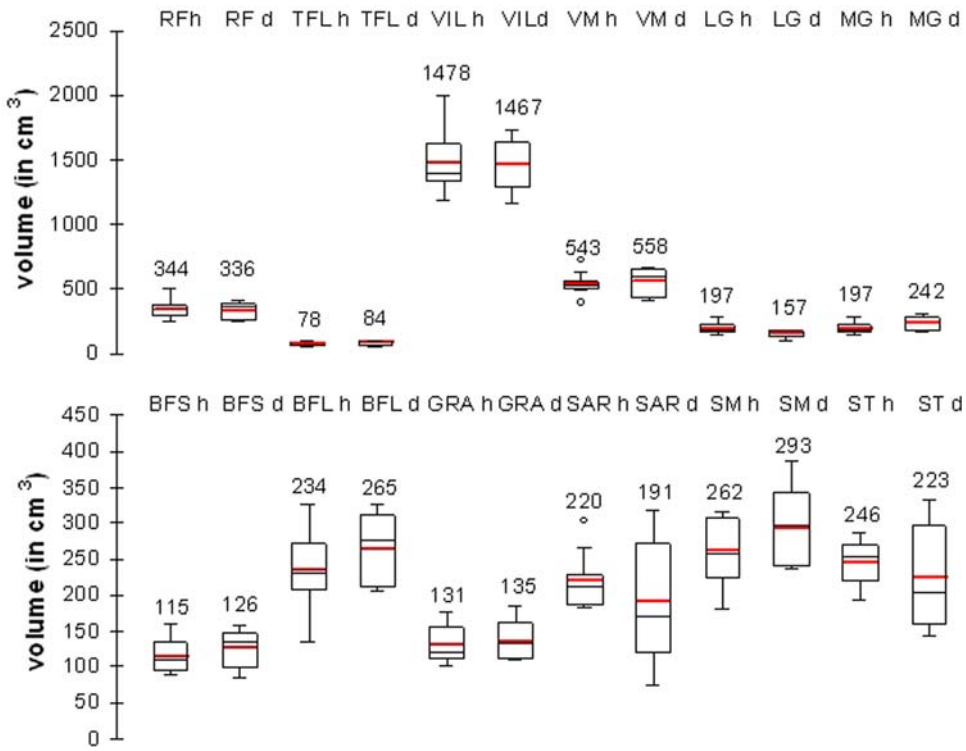

Fig. 4 Volume of the muscles (in cubic centimeter) for ten asymptomatic (*h*) and five ACLD (*d*) subjects. The mean value is indicated. The lower and upper limits of each *box* represent the first and third quartile

reconstructions for most of the muscles (10% for the smaller ones, 24% for the LG). These values can be mainly explained by the difficulty to identify precisely the muscles (especially the *gastrocnemii*) on the slices and are similar to the errors reported in the literature. Jolivet et al. [13] computed the volume of the reconstructions of hip muscles of 30 subjects made by three operators. They reported an error (two standard deviations around the mean volume) of 5–12%. Eng et al. [8] reported a mean error of 9% between the volumes of forearm muscles reconstructed by two operators. The reproducibility of the shape of the reference models was very good (point-surface errors within 3 mm).

The volume reproducibility was slightly inferior to the one obtained for the reference models: mean error ranged

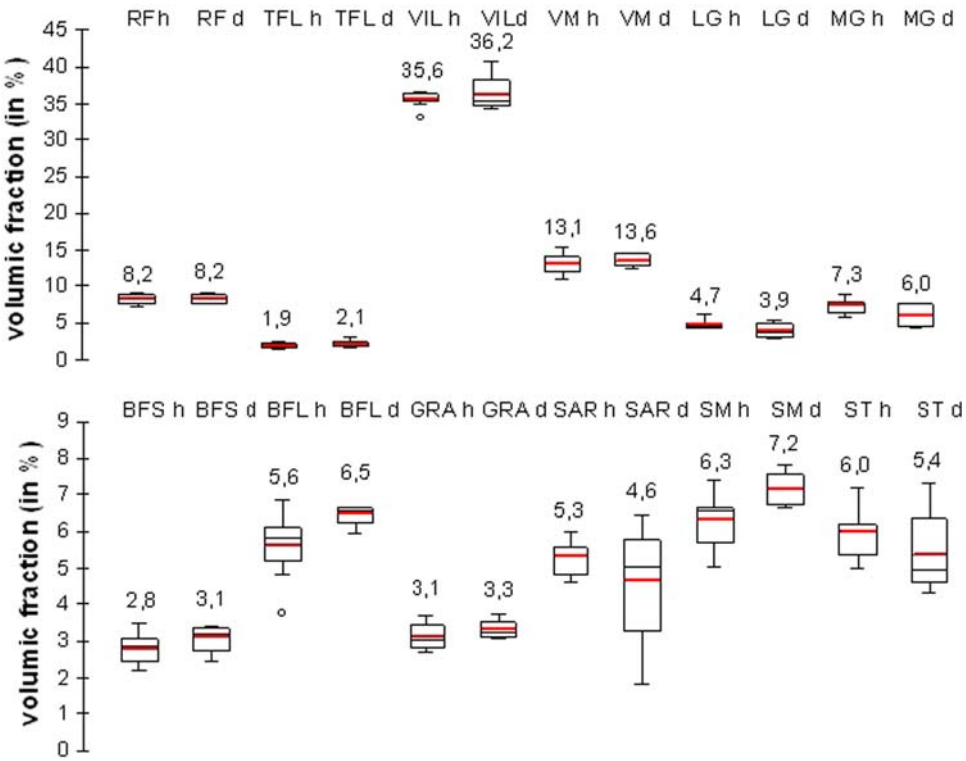

Fig. 5 Volumic fraction of the muscles (in percent of the global volume) for ten asymptomatic (*h*) and five ACLD (*d*) subjects. The mean value is indicated. The lower and upper limits of each *box* represent the first and third quartile

Table 3 Mean and standard deviations of absolute differences in slices obtained by the two operators for the lower limit (LL) and the higher limit (HL)

	BFS	BFL	RF	LG	MG	GRA	SAR	SM	ST	TEL	VIL	VM
LL (slices)												
Mean	2.4	1.3	0.7	1.9	2.4	2.0	1.8	1.7	1.2	1.2	3.4	1.7
2SD	4.2	2.0	2.0	3.0	2.6	3.0	3.2	2.0	1.6	1.4	2.8	2.6
HL (slices)												
Mean	1.9	2.1	1.0	1.8	2.1	1.0	2.9	1.4	0.7	1.6	2.1	1.9
2SD	3.0	2.8	1.8	2.4	3.8	1.8	3.4	1.8	1.0	2.0	3.2	2.4
Volume error (%)												
Mean	2.1	0.5	0.3	1.6	1.4	0.7	1.6	0.7	0.2	1.9	0.7	1.2
2SD	4.4	0.5	0.6	2.1	2.3	0.8	1.7	1.0	0.3	2.9	0.6	2.4

The volume error (with respect to the volume obtained using reference models) due to the error in LL and LH is also presented in the last line as mean and standard deviations (SD)

from 2 to 11% depending on the muscles, while standard deviations remained below 5.3% (except for LG). As for the reference models, larger relative volume reproducibilites were found for smaller muscles like BFS, SAR, and GRA. Considering the point-surface errors, the reproducibility of our protocol was good (global 2RMS <3 mm, except for the *gastrocnemii*).

4.3 Preliminary clinical research application

The volume of the biceps femoris and SM was 10% higher for the ACLD subjects compared to the asymptomatic population, while the opposite was observed for the SAR and ST. The total muscle volume of quadriceps and hamstrings of the asymptomatic subjects in the present study (mean of about 2,360 and 900 cm^3 respectively) were higher than those reported in the literature [14, 22, 25]. Konishi et al. obtained a mean quadriceps volume of 1,500 cm^3, Williams et al. obtained mean quadriceps and hamstrings volumes of 1,800 and 600 cm^3, while Morse et al. obtained a mean quadriceps volume of 2,040 cm^3. The smaller volume obtained by Konishi et al. can be explained by the fact that only the 70% most distal part of the thigh was studied because of the difficulty to

differentiate muscles in the proximal part of the thigh. The smallest values obtained by Williams et al. could be partly due to the considered population (two women, seven men). Morse et al. considered 18 young men and obtained similar values to ours. Moreover, as opposed to those authors, we did not observe any quadriceps atrophy for our ACLD patients. However, more subjects need to be studied to verify this result, the aim of this preliminary study being mainly to highlight the potential of DPSO muscle volume reconstruction method to analyze the entire muscle system of lower limb.

The described method does not take into account very local geometric deformities, as the maximal distance between two slices reached 6 cm. A simple solution to take such deformities into account would be to visually verify the quality of the superimposition of the muscle model on MRI and, if needed, add locally some manual contours to improve the quality of the reconstruction.

Previous studies have assessed the consistent distribution of muscles at the hip [13] and in the upper limb [10]. Our study confirmed this consistency for the muscles involved in the knee joint motion, as the volumic fractions differed by less than 1% between ACLD and asymptomatic subjects. The deviation of those fractions was small, except for the SAR, MG and VIL muscles of ACLD patients.

5 Conclusion

The DPSO method used in the present study provides the entry data for patient-specific musculoskeletal models. As the patient-specific muscle geometry is easy and fast to obtain, this method can be applied to a wide population. The next step will consist in integrating this muscular geometry to the geometry of the bones, obtained for instance through stereoradiographic acquisitions with the low-dose EOS® system, and to motion analysis. Combining muscular geometry, force, and functional evaluations, kinematics and kinetics, and setting up patient-specific musculoskeletal models, will be very helpful to better understand the complex locomotor system.

Acknowledgments We thank D. Blain, N. Langlois (Radiological Department, University of Montreal Hospital Centre), and M. Charbonneau (LIO, Montreal) for their help in MRI acquisitions. We also thank Pr J.D. Laredo for helpful comments. This work was funded by the Canada Research Chair in 3D Imaging and Biomedical Engineering, Chaire de recherche en orthopédie Marie-Lou et Yves Cotrel du CHUM, the MENTOR program (ETS-IRSC), and the EGIDE program (Ministère des affaires étrangères français, Ministère des relations internationales québécois).

Conflict of interest statement None declared.

References

1. Aagaard P, Andersen JL, Dyhre-Poulsen P et al (2001) A mechanism for increased contractile strength of human pennate muscle in response to strength training: changes in muscle architecture. J Physiol 534(Pt 2):613–623. doi:10.1111/j.1469-7793.2001.t01-1-00613.x
2. Arangio GA, Chen C, Kalady M et al (1997) Thigh muscle size and strength after anterior cruciate ligament reconstruction and rehabilitation. J Orthop Sports Phys Ther 26(5):238–243
3. Arnold AS, Salinas S, Asakawa DJ et al (2000) Accuracy of muscle moment arms estimated from MRI-based musculoskeletal models of the lower extremity. Comput Aided Surg 5(2):108–119
4. Asakawa DS, Blemker SS, Rab GT et al (2004) Three-dimensional muscle-tendon geometry after rectus femoris tendon transfer. J Bone Joint Surg Am 86-A(2):348–354
5. Blemker SS, Asakawa DS, Gold GE et al (2007) Image-based musculoskeletal modeling: applications, advances, and future opportunities. J Magn Reson Imaging 25(2):441–451. doi:10.1002/jmri.20805
6. Blemker SS, Delp SL (2005) Three-dimensional representation of complex muscle architectures and geometries. Ann Biomed Eng 33(5):661–673. doi:10.1007/s10439-005-1433-7
7. Cordier F, Magnenat-Thalmann N (1998) Comparison of two techniques for organ reconstruction using visible human dataset. In: Second visible human project conference. National Library of Medicine, Bethesda, 1–2 Oct 1998. http://www.nlm.nih.gov/research/visible//vhpconf98/AUTHORS/CORDIER/FULLTEXT.HTM
8. Eng CM, Abrams GD, Smallwood LR et al (2007) Muscle geometry affects accuracy of forearm volume determination by magnetic resonance imaging (MRI). J Biomech 40(14):3261–3266. doi:10.1016/j.jbiomech.2007.04.005
9. Holzbaur KR, Delp SL, Gold GE et al (2007) Moment-generating capacity of upper limb muscles in healthy adults. J Biomech 40(11):2442–2449. doi:10.1016/j.jbiomech.2006.11.013
10. Holzbaur KR, Murray WM, Gold GE et al (2007) Upper limb muscle volumes in adult subjects. J Biomech 40(4):742–749. doi:10.1016/j.jbiomech.2006.11.011
11. Hopkins WG (2000) Measures of reliability in sports medicine and science. Sports Med 30(1):1–15. doi:10.2165/00007256-200030010-00001
12. Jolivet E (2007) Modélisation biomécanique de la hanche dans le risque de fracture du fémur proximal. In: Laboratoire de biomécanique. Ecole Nationale Supérieure d'Arts et Métiers, Paris, p 178
13. Jolivet E, Daguet E, Pomero V et al (2008) Volumic patient-specific reconstruction of muscular system based on a reduced dataset of medical images. Comput Methods Biomech Biomed Eng 11(3):281–290. doi:10.1080/10255840801959479
14. Konishi Y, Ikeda K, Nishino A et al (2007) Relationship between quadriceps femoris muscle volume and muscle torque after anterior cruciate ligament repair. Scand J Med Sci Sports 17(6):656–661
15. Lampe R, Grassl S, Mitternacht J et al (2006) MRT-measurements of muscle volumes of the lower extremities of youths with spastic hemiplegia caused by cerebral palsy. Brain Dev 28(8):500–506. doi:10.1016/j.braindev.2006.02.009
16. Lloyd DG, Besier TF (2003) An EMG-driven musculoskeletal model to estimate muscle forces and knee joint moments in vivo. J Biomech 36(6):765–776. doi:10.1016/S0021-9290(03)00010-1
17. Makihara Y, Nishino A, Fukubayashi T et al (2006) Decrease of knee flexion torque in patients with ACL reconstruction: combined analysis of the architecture and function of the knee flexor muscles. Knee Surg Sports Traumatol Arthrosc 14(4):310–317. doi:10.1007/s00167-005-0701-2

18. Malaiya R, McNee AE, Fry NR et al (2007) The morphology of the medial gastrocnemius in typically developing children and children with spastic hemiplegic cerebral palsy. J Electromyogr Kinesiol 17(6):657–663. doi:10.1016/j.jelekin.2007.02.009
19. Mikosz RP, Andriacchi TP, Andersson GB (1988) Model analysis of factors influencing the prediction of muscle forces at the knee. J Orthop Res 6(2):205–214. doi:10.1002/jor.1100060207
20. Mitton D, Landry C, Veron S et al (2000) 3D reconstruction method from biplanar radiography using non-stereocorresponding points and elastic deformable meshes. Med Biol Eng Comput 38(2):133–139. doi:10.1007/BF02344767
21. Mitulescu A, Semaan I, De Guise JA et al (2001) Validation of the non-stereo corresponding points stereoradiographic 3D reconstruction technique. Med Biol Eng Comput 39(2):152–158. doi:10.1007/BF02344797
22. Morse CI, Degens H, Jones DA (2007) The validity of estimating quadriceps volume from single MRI cross-sections in young men. Eur J Appl Physiol 100(3):267–274. doi:10.1007/s00421-007-0429-4
23. Pomero V, Vital JM, Lavaste F et al (2002) Muscular modelling: relationship between postural default and spine overloading. Stud Health Technol Inform 88:321–325
24. Trochu F (1993) A contouring program based on dual kriging interpolation. Eng Comput 9:160–177. doi:10.1007/BF01206346
25. Williams GN, Buchanan TS, Barrance PJ et al (2005) Quadriceps weakness, atrophy, and activation failure in predicted noncopers after anterior cruciate ligament injury. Am J Sports Med 33(3):402–407. doi:10.1177/0363546504268042
26. Williams GN, Snyder-Mackler L, Barrance PJ et al (2005) Quadriceps femoris muscle morphology and function after ACL injury: a differential response in copers versus non-copers. J Biomech 38(4):685–693. doi:10.1016/j.jbiomech.2004.04.004
27. Zajac FE, Neptune RR, Kautz SA (2003) Biomechanics and muscle coordination of human walking: part II: lessons from dynamical simulations and clinical implications. Gait Posture 17(1):1–17. doi:10.1016/S0966-6362(02)00069-3